MODELS FOR THE FREQUENCY DEPENDENCE OF ULTRASONIC SCATTERING FROM REAL FLAWS

Laszlo Adler and Kent Lewis
University of Tennessee
Knoxville, Tennessee 37916

My objective is to help develop a quantitative working model for a typical nondestructive testing system. Specifically, our objective is to relate the parameters which characterize a defect such as size, orientation, and shape to the ultrasonic scattering field parameters such as amplitude, frequency, scattering angle, and polarization or mode conversion. In Fig. 1 is shown a flat surface sample immersed in liquid containing a real flaw a certain distance below the surface; i.e., in the bulk of the material. Sound waves propagate through the liquid and for the simplest case the wave front enters such that only incident longitudinal waves are present. The waves at the flaw are scattered, and also mode converted; the scattered wave, which will now be both shear and longitudinal will be reconverted back to a longitudinal wave once leaving the solid body and picked up by a receiver oriented at some angle.

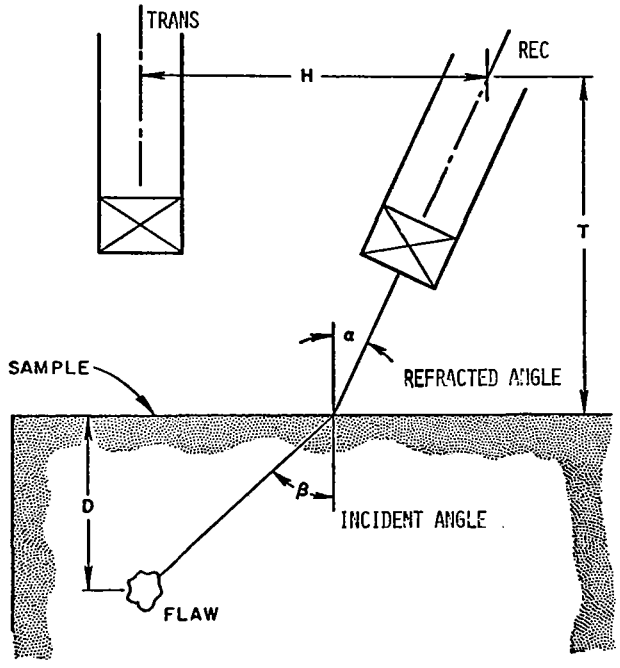

Figure 1. Typical NDE system to characterize real flaws by elastic wave scattering.

We received diffusion bonded samples from the Rockwell International Science Center for our investigation. These were titanium samples, disks 4 in. in diam. and 2 in. thick and various types of cavities were at the center. These cavities were in two basic categories: (1) circular and elliptical crack-like disks, and (2) spheroidal type of cavities. The first group models crack-like flaws and the second group would be more like a void type of flaw. The oblate spheroid, when it is smashed, will also approach the crack-like flaw.

There is another difference between the two groups of cavities. For the crack-like flaws, that is for the disks, the dimensions ranged from about 1200 μm to 5,000 μm in diam., and for the spheroidal defects, the dimensions were as small as 100 μm. So, we are dealing with problems that from a scattering point of view are ranging from something like ka = 0.1 to about ka = 20.

In order to make a quantitative evaluation we searched for existing studies to evaluate our experiments. There is not really one single theory which would cover the range from ka much less than 1 to ka much larger than 1. For ka less than 1 or equal to 1 we used the Born approximation developed at Cornell by Krumhansl, Gubernatis and Domany. For the large size defects, especially with sharp edges and for the circular and elliptical disk cavities, we used Keller's theory which originally was developed for diffraction of electromagnetic waves, and we applied it to scalar acoustic waves.

I should say a few words about this theory. As I mentioned, Keller introduces the concept of diffracted rays in his theory. When you have an edge of some sort, contrary to geometrical theory for acoustics or optics in which only incident reflected and refracted waves are considered, diffracted rays are produced any time a ray hits an edge. Figure 2 shows these diffracted rays. They describe a cone. The angle for the diffracted rays from the edge is the same as the incident.

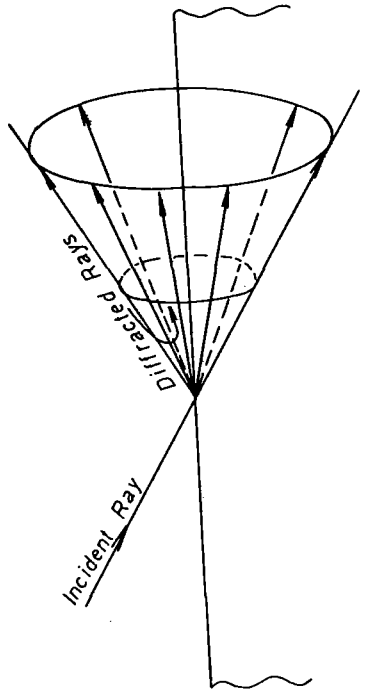

Figure 2. Schematic diagram of "Ray" diffraction from edges.

Generalizing the Fermat principle to a bonded and a discontinuous medium is another way to treat the problem.

The advantage of this theory is that in addition to having qualitative information through ray tracing, some field and phase values are assigned to the incident waves. One can actually make some quantitative calculations of the incident field. The incident field is related to the diffracted field through the diffraction coefficient. The diffraction coefficients are evaluated from the exact theory using some kind of asymptotic expansion of exact theory to get the result for the semi-infinite plane as solved by Sommerfield.

Keller points out that although the result originally was intended for ka larger than 1, it works surprisingly well for ka equal to 1. This is in the region of our interest.

Let me give you one expression here. This is for the complex amplitude of the diffracted field at any given point due to an arbitrary shaped two-dimensional scatterer. Let me point out some of these parameters. We have a summation for the number of diffracted rays. A(k) is the incident amplitude in k space. The important parameters are all geometrical.

$$U = \sum \frac{Ae^{ik(\psi+s)+\frac{i\pi}{4}}}{2(2\pi k)^{\frac{1}{2}}\sin\beta x}\left[\sec\tfrac{1}{2}(\theta-\alpha)\right] \pm \csc\tfrac{1}{2}(\theta+\alpha)\Big] x$$

$$\left[s\left(1-\frac{s\left[\cos\delta+\rho\dot{\beta}\sin\beta\right]}{\rho\sin^2\beta}\right)\right]^{-1/2} \qquad (1)$$

In Figure 3 the symbols are explained.

β is the angle between the incident ray and the tangent to the aperture. It will depend on both the geometry of the scatterer as well as the direction of the incident ray. For normal incidence it's fairly simple, but for oblique incidence, the value of β will depend on several factors.

$\dot{\beta}$ from the previous equation is the derivative of this β with respect to the arc length. For a scatterer with complicated shape, the problem is fairly complex, but it can be handled for a two-dimensional scatterer having any shape.

For a circular scatterer, the expression we obtain for the general case of any oblique incident wave is expressed in fairly simple form

$$U = A(k)_1\sqrt{\frac{2}{k(\sin\theta+\sin\alpha)}}\left[\frac{\sin^2[ka(\sin\theta+\sin\alpha)-\frac{\pi}{4}]}{\sin^2(\frac{\theta+\alpha}{2})} + \frac{\cos^2[ka(\sin\theta+\sin\alpha)-\frac{\pi}{4}]}{\cos^2(\frac{\theta-\alpha}{2})}\right]^{1/2} \qquad (2)$$

where α is the incident angle and θ is the diffracted angle; A(k) is the amplitude distribution of the incident wave and is characteristic of the transducer. This expression can be used for both the pulse echo technique and for the pitch-catch method. The incident beam is perpendicular to the scatterer. In this case $\alpha = 0$ and the expression simplifies.

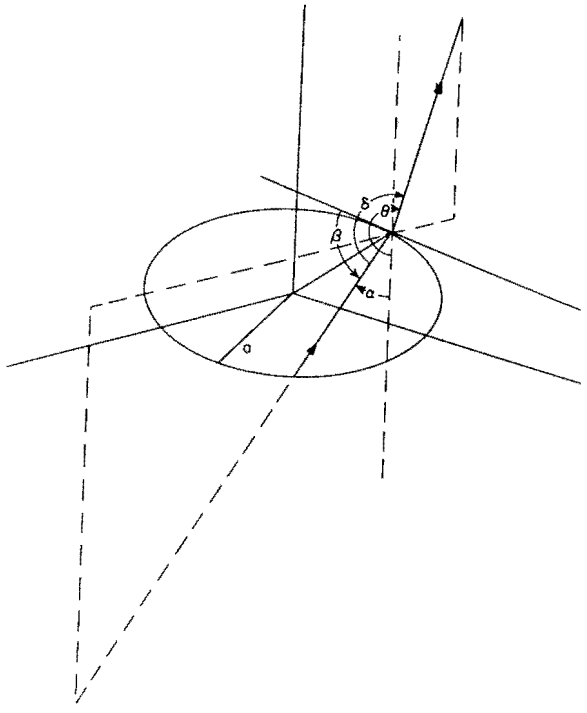

Figure 3. Diffraction of ray from aperture.

The two variables, the frequency F and the scattered angle θ, are the ones which we tried to correlate to the size of the scatterer and this is calculated from Eqn. (2) for the 1200 μm diam. penny-shaped cavity inside titanium as shown in Fig. 4. The scattered angle varies from 30° to about 70° and the frequency varies from about 2 to 6 MHz. This is the frequency range in our investigation.

We made some calculations for the case where the scattered wave mode is converted into a shear wave. The calculations for the scattered shear wave are shown in the same figure.

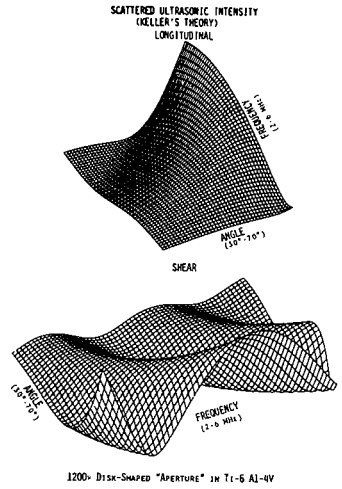

Figure 4. Calculated intensity distribution for a 1200μ disk-shaped aperture (Keller's theory).

For a 5000 μm diam. disk the result is shown in Fig. 5. The larger the size of the defect, the more detail is obtained in the frequency spectrum. In the angular dependence there is also more detail for the larger size cavity than for the smaller cavity.

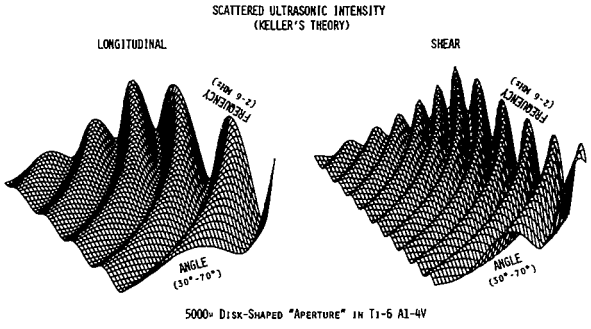

Figure 5. Calculated intensity distribution for a 5000μ disk-shaped aperture (Keller's theory).

The other type of crack-like defect was an elliptical disk inside titanium and we made calculations for the elliptical case from Keller's theory.

$$U(p) = \frac{A(k)\rho\ (\psi)}{\sin\phi}\ \frac{1-\cos\phi\sin 2(ka(\psi)\sin\phi}{k\rho\ (\psi)\sin\phi}^{1/2} \qquad (3)$$

where

$$a(\psi) = \varepsilon b[1 + (\varepsilon^2 - 1)\ (1+ \varepsilon^2\tan^2\psi)^{-1}\ ]^{-1/2}$$

$$\rho\ (\psi) = \varepsilon^{-1} b\ [\ 1 + (\varepsilon^2-1)(1 + \varepsilon^2\tan^2\psi)^{-1}]^{3/2}.$$

Equation (3) applies to the case of normal incidence for longitudinal waves. The basic difference between Eqn. (2) and Eqn. (3) is an additional parameter ψ, which is the angle in the plane of ellipse.

Figure 6 shows the calculated scattering pattern as a function of frequency and projection angle ψ for a fixed scattering angle for a 1200μmx 5000μm elliptical aperture in titanium. The separation of the frequency maxima along the major and minor axes are the same as the pattern for the corresponding circular aperture of the same size but there is a change in the relative intensities. The pattern change in ψ indicates that there is an asymmetrical discontinuity. No such variation is present for a circular discontinuity.

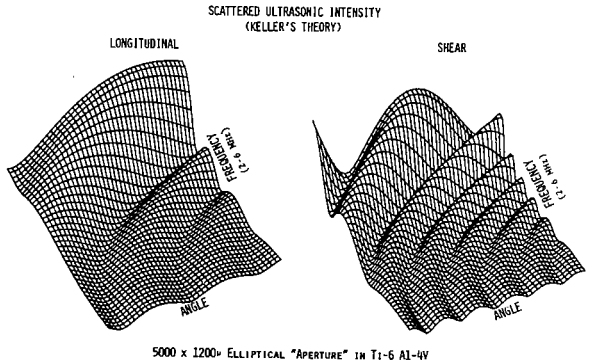

Figure 6. Calculated intensity distribution for a 5000μ x 1200μ elliptical aperture (Keller's theory) shown as a function of projection angle ψ for a fixed scattering angle of 45°.

In Fig. 7 is shown a schematic idagram of our experimental setup. A ceramic transducer is shock excited, producing a broadband spectrum. This pulse propagates through the water-titanium interface and interacts with the cavity. The scattered pulse (which is now both shear and longitudinal) through the titanium-water interface (the shear wave is mode converted in water) and is received by a second broadband transducer. The signal is amplified, gated out, and spectrum analyzed. Figure 8 is a picture of the experimental setup.

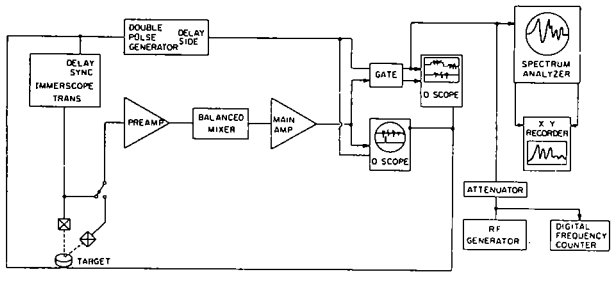

Figure 7. Experimental arrangement.

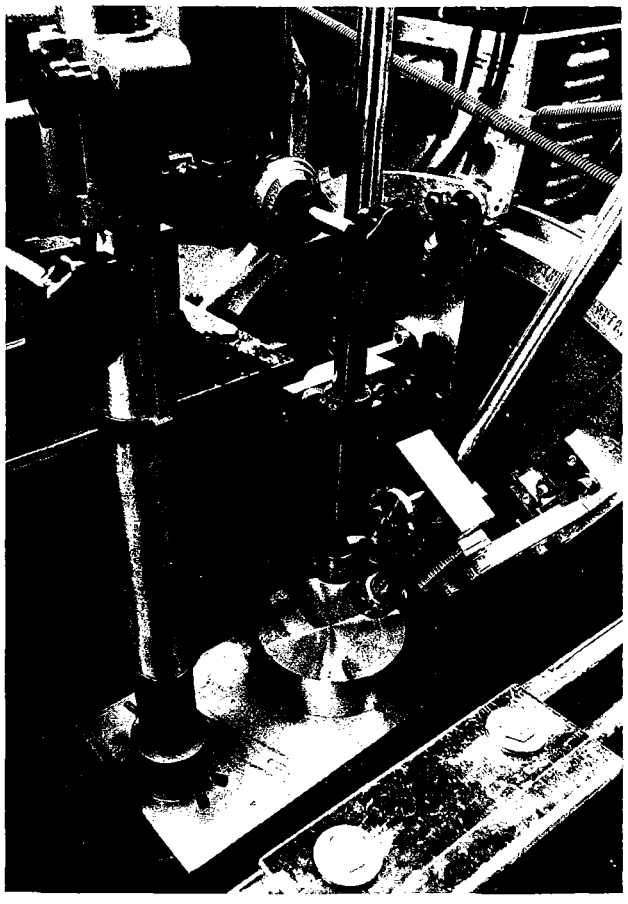

Figure 8. Mechanical System.

Since both Keller's theory and the Born approximation theory are valid for an infinitely extended solid, we had to make corrections due to the interface. We calculated the transmission curve for the shear and for the longitudinal wave coming out from a titanium sample in water (Fig.9) These corrections were applied to our data.

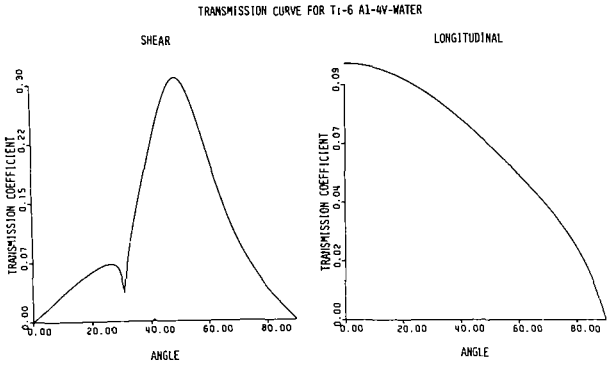

Figure 9. Transmission curve for titanium-water.

Scattering experiments were carried out for the 1200 μm and 5000 μm diameter circular shaped cavities in titanium for various scattering angles. Experiments were done also for the 1200 μm x 5000μm epplitical cavity. The condensed result is shown for the longitudinal scattering in Fig. 10 in the case of the 5000 μm cavity for four different scattering angles. The solid line is calculated from Keller's theory. The agreement is quite good. The agreement is also good for the elliptical disk shown in Fig. 11.

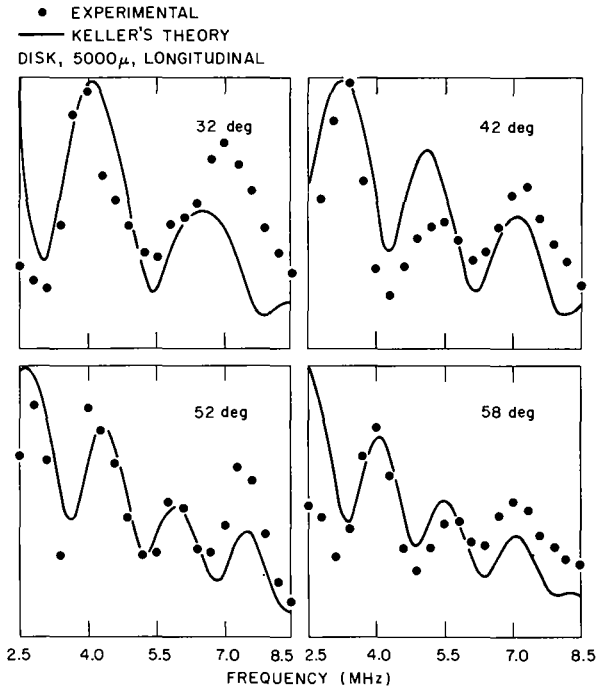

Figure 10. Comparison between experimental and Keller's theory for the intensity of longitudinal scattered wave as a function of frequency for a 5000μ thin disk-shaped cavity embedded in tianium.

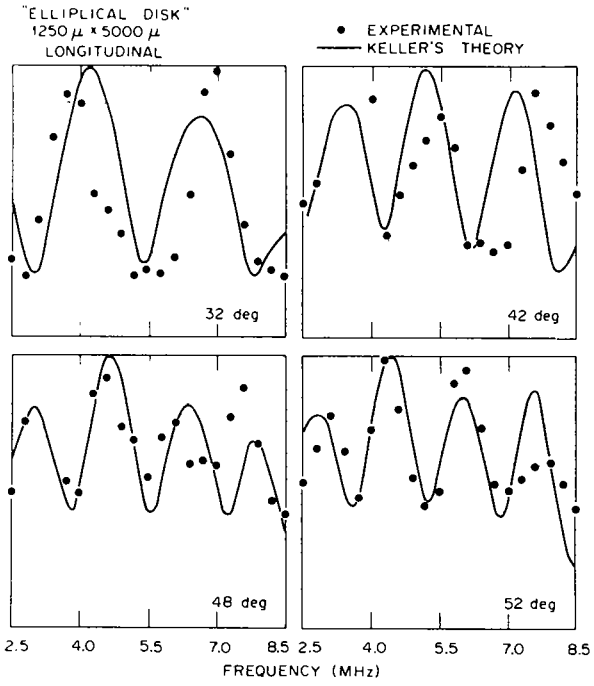

Figure 11. Comparison between experiment and Keller's theory for the intensity of longitudinal scattered wave as a function of frequency for a 1250μ x 5000μ thin elliptical disk-shaped cavity embedded in titanium.

In the next set of experiments, we investigated elastic waves scattering from spheroidal cavities in titanium. Three cavities were studied: an oblate spheroid of dimensions 400 x 800 μm (diameters), the 800 μm diam. sphere, and the 1600 μm x 800 μm prolate spheroid. For an incident longitudinal wave at normal incidence the scattered frequency spectrum was recorded for several scattered angles. The scattered shear and longitudinal waves were separately analyzed. In the theoretical analysis the Born approximation was used. Figures 12, 13, and 14 are three-dimensional plots of calculations using the Born approximation for the three cavities. The frequency and angular dependence of the scattered power is plotted for the range of our experiment. Clearly there are distinct features of both the scattered shear and longitudinal waves with cavities' shape and/or size obtainable from the Born approximation theory. The theory compares well with experiment for the oblate spheroid (Fig. 15). For the sphere (Fig. 16) and prolate spheroid (Fig. 17) the agreement is only fair. One would expect that, since the ka is about 0.1 to 0.8 for the oblate spheroid but is up to ka $\simeq$ 10 for the prolate spheroid (for shear waves at 8 MHz) and the Born approximation really works better for small ka.

In conclusion, I would like to point out that all these experiments were carried out using normal incidence and pitch-catch techniques. We are also planning to do some work using the oblique incidence to the surface. This, of course, will introduce additional problems because both incident shear and longitudinal waves will be present.

We would like to extend Keller's theory to other than plane geometry. It seems to me that it would be somewhat useful to have the ray approach for focussed transducers and for other than flat surfaces. The theory should also be extended to elastic problems.

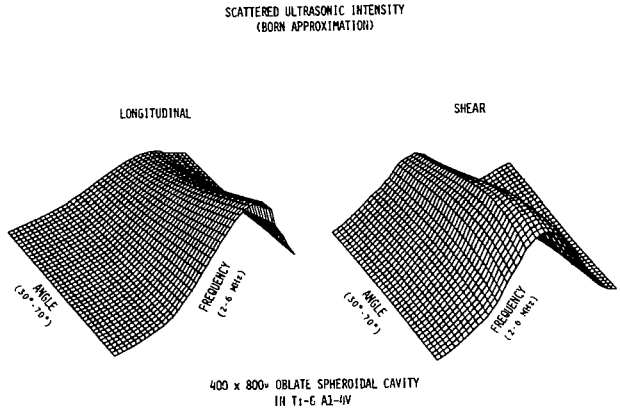

Figure 12. Calculated intensity distribution for a 400μ x 800μ oblate spheroid cavity in titanium (Born approximation).

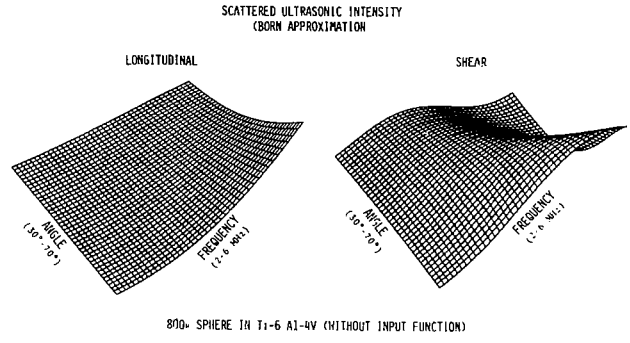

Figure 13. Calculated intensity distribution for a 800μ spherical cavity in titanium (Born approximation).

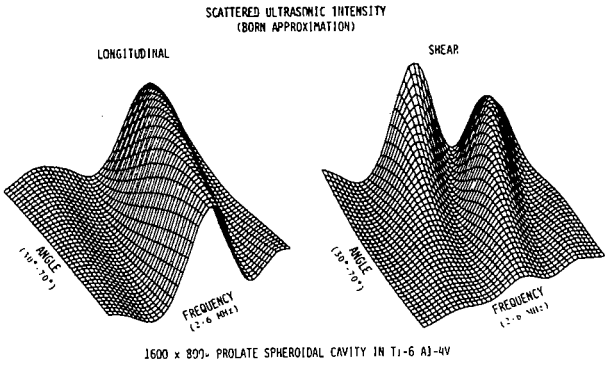

Figure 14. Calculated intensity distribution for a 1600μ x 800μ prolate spheroid cavity in titanium (Born approximation).

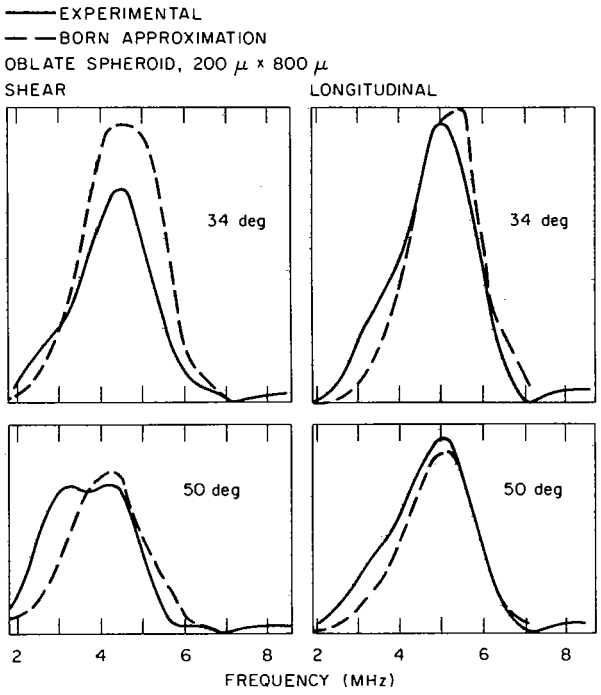

Figure 15. Comparison of experiment to Born approximation for the intensity of scattered waves spectra for a 200μ x 800μ oblate spheroid cavity embedded in titanium.

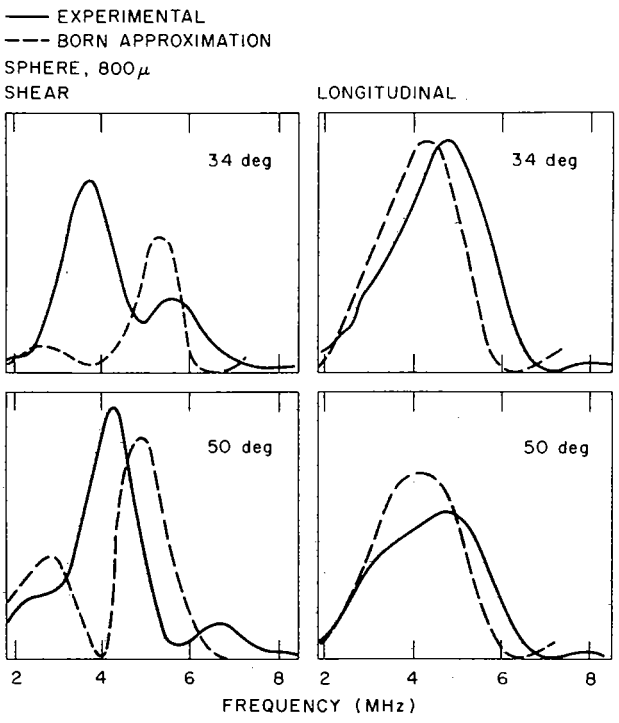

Figure 16. Comparison of Experiment to Born approximation for the intensity of scattered waves spectra for a 800μ spherical cavity embedded in titanium.

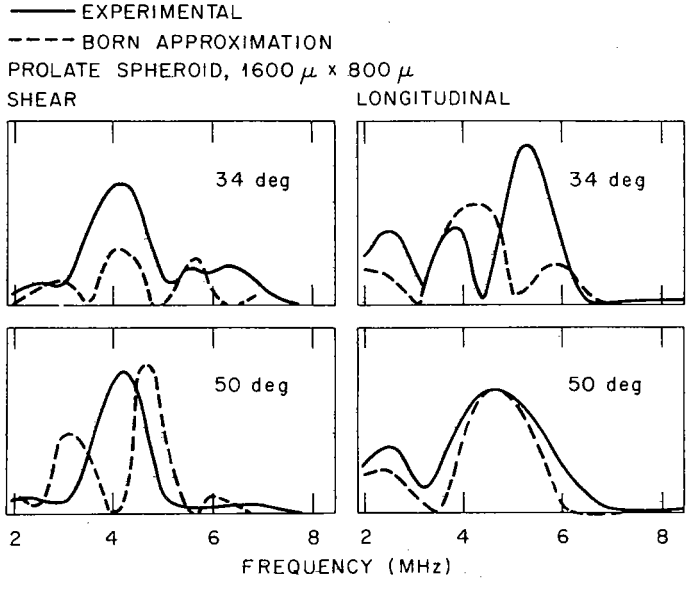

Figure 17. Comparison of experiment to Born approximation for the intensity of scattered waves spectra for a 1600μ x 800μ prolate spheroid cavity embedded in titanium.

DR. EMMANUEL PAPADAKIS (Ford Motor Company): Thank you, Laszlo. May I ask you to save your questions for him for coffee break.